High-Resolution CT Images Yield Accurate Microstructural Information if Processed by 3D Extensions of Standard Histomorphometric Analysis of Fuzzy Segmentation Approaches

A. Krebs[1], C. Graeff[1], I. Frieling[2], B. Kurz[3], W. Timm[4], C.-C. Glüer[1]

[1]Medical Physics, Dep. of Diagnostic Radiology, Univ. Clinic Schleswig-Holstein, Campus Kiel, Germany; [2]Osteoporose-Praxis Neuer Wall, Hamburg, Germany; [3]Anatomisches Institut, CAU, Kiel, Germany; [4]Synarc, Hamburg, Germany

Introduction

Monitoring of osteoporosis therapy based solely on bone densitometry is insufficient to assess anti-fracture efficacy. Microstructure of trabecular bone represents an additional aspect of bone quality that affects bone strength indepent of BMD. Bone biopsies, high-resolution MRI, or dedicated (pQCT) imaging systems for measurement in peripheral regions of the skeleton such as forearm or tibia provide an insight into the microstructure and show trabecular distances varying between 500–2000 μm. As can be expected because of the different loading conditions, structural measures from biopsies and peripheral sites show limited correlations with the clinically important fracture sites proximal femur and vertebrae.

In vivo assessment of trabecular bone microstructure is bounded by image quality and radiation exposure. We investigate whether microstructural information can be accurately extracted from high-resolution CT (HRCT) images of human vertebrae.

Methods

The microstructural variables *BV/TV* (bone volume / total volume), *Tb.Th* (trabecular thickness), and *Tb.Sp* (trabecular separation) can be defined by 3-D adaptation of 2-D stereological methods used in histomorphometry. A. LAIB and P. RÜEGSEGGER introduced comparable measures *Tb.Th** and *Tb.Sp** which assess metric distances in 3D space directly. When moving from μCT measurements with cubic voxels of 28 μm sidelength to HRCT measurements with cubic voxels with sidelength 165 μm these distance based measures showed higher correlations than the stereologically motivated measures (cf. [LR99, Table 3]).

The bottom and middle plots of Fig. 1 show what happens to the histograms of vertebra images when moving from μCT to HRCT measurements: Due to partial volume effects and noise the bone peak melts into the mark peak and the bone/mark binarization becomes an issue.

Fuzzy segmentation approaches may overcome these limitations. A sigmoidal *membership function* maps the voxel's gray value onto the $[0;1]$ interval (cf. top plot of Fig. 1). The assigned value represents the probability of the voxel to be bone. The concept of *fuzzy distance* allows probability weighted measurement of distances: A 2 mm long line of voxels with a membership value 1 leads to a fuzzy distance of 2 mm. If the same line consists of voxels with a membership value 0.3, this yields a fuzzy distance of $0.3 \cdot 2$ mm = 0.6 mm.

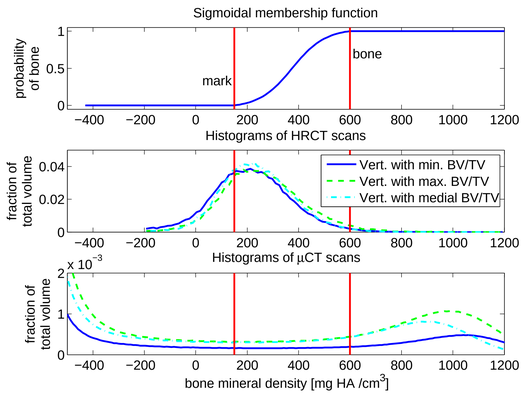

Figure 1: Histograms of three vertebra images from Set 1, namely of the vertebrae with maximal, minimal, and medial BV/TV. The discrimination bone versus mark becomes unclear when moving from μCT images (bottom) to HRCT images (middle). The membership function (top) assigns a probability value from $[0,1]$ to each voxel according to its BMD value.

The *fuzzy distance transformation* (FDT) assigns to every potential bone voxel (membership value > 0) the shortest weigthed distance to the mark background (membership value $= 0$) (cf. [SW04]). The skeletonization of the bone phase based on the *fuzzy distance transformation* permits the direct measurements of trabecular thickness Tb.Th^F and separation Tb.Sp^F comparable to the directly distance measured variables Tb.Th* and Tb.Sp* proposed in [LR99]).

Measurements: 16 vertebral biopsies of 8 mm diameter and 9 mm height (Set 1) were measured by HRCT (Siemens Somatom 16, 120 kV, 360 mAs, pixel size 156×156 μm^2, slice thickness 400 μm) inside a CIRS abdomen phantom with tissue equivalent lumbar section to emulate in vivo conditions. Additionally, using the same HRCT protocol, 15 whole vertebrae embedded in PMMA (Set 2) were measured inside the phantom surrounded by an additional attenuator ring to simulate obese patients (see Fig. 2).

Reference measurements on micro-CT systems were obtained on a Scanco μCT40 (voxel size 24^3 μm^3) for Set 1 and a Scanco Xtreme CT (XCT) (voxel size 82^3 μm^3) for Set 2.

All image processing was performed using the software `StructuralInsight V1.48` and its `FDT Add-on` developed in-house. For the biopsies of Set 1, volume of interest was determined by applying a cylindrical mask containing the biopsy completely. μCT data was accepted as calibrated to [mg HA/cm^3] according to machine output, HRCT data was calibrated with respect to a reference reconstruction of the scan containing the calibration phantom (cf. Fig. 2 (left)).

For the vertebrae of Set 2, the complete trabecular bone volume was segmented excluding hyperdense degenerative calcifications and the thin cortical rim of the vertebral body. The masking was based on polygons manually defined by the user in multiple, nonadjecent slices). The reference measurements were adjusted to [mg HA/cm^3] by the XCT calibration procedure, HRCT data with reference to the calibration phantom.

Results

Fig. 3 displays a detail of an unfiltered sagital cut through a vertebra of Set 2, the same detail after a sampling to HRCT resolution 156×156 × 400μm^3(b), and the FDT of the sampled image (c).

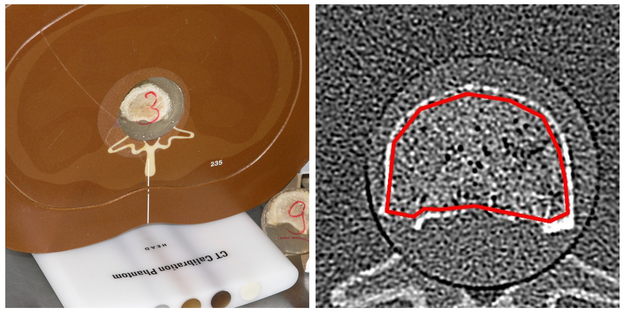

Figure 2: Left: PMMA embedded vertebra in CIRS model 235 abdominal phantom (brown) with the attenuator ring to simulate obese patients. Five rods of reference material embedded in the CT calibration phantom (white) permit the conversion of the image's grayvalues to BMD in [mg HA/cm^3]. Right: HRCT reconstruction. The trabecular bone was segmented based on manually defined polygons (red) excluding cortical rim.

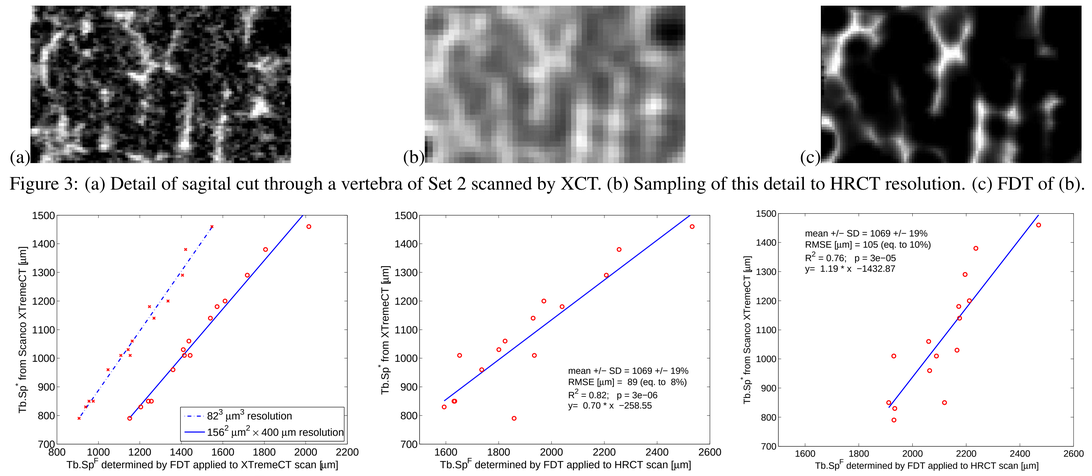

Figure 3: (a) Detail of sagital cut through a vertebra of Set 2 scanned by XCT. (b) Sampling of this detail to HRCT resolution. (c) FDT of (b).

Figure 4: Tb.Sp* versus Tb.Sp^F correlations for PMMA embedded vertebrae of Set 2. Left: The reference (mean $\pm$SD $= 1069 \pm 19\%$) can be predicted by $\text{Tb.Sp}^* = 1.096 \cdot \text{Tb.Sp}^F - 20\,\mu\text{m}$ with a root mean square error (RMSE) of 40 μm (3.7% of the mean of response), $R^2 = 0.96$, and $p < 10^{-9}$ for the original images. For the lower resolution images the prediction follows $\text{Tb.Sp}^* = 0.732 \cdot \text{Tb.Sp}^F - 96\,\mu\text{m}$ with RMSE $= 26$ μm (2.4%), $R^2 = 0.98$, and $p < 10^{-12}$. Middle: Using HRCT images scanned *without* the CIRS abdominal phantom (see Fig. 2) yields the displayed results. Right: Results for the scans taken *with* the abdominal phantom.

Validation: The FDT based analogon Tb.Sp^F of Tb.Sp* was calculated for the 15 vertebra images of Set 2 scanned by XCT. Additionally, Tb.Sp^F was calculated for 15 images yielded by sampling the XCT images to HRCT resolution 156×156 × 400μm^3. The results for both resolutions are plotted in Fig. 4 (left). Using best line regression, the reference values Tb.Sp* can be predicted as given in the figure's caption. For the original images, the deviation Tb.Sp* - Tb.Sp^F can be explained by the different determination of the volume of interest: XCT uses semi-automatic masking, `Structural Insight` demands manual masking by polygons (see above).

Application to HRCT images: The middle and right plot of Fig. 4 show higly significant regression results for Tb.Sp^F from HRCT images taken *without* and *with* the body phantom, respectively. Table 1 lists the linear regression results for the variables BV/TV, Tb.Th*, and Tb.Sp* versus the respective stereologic variables (cf. [GTN+07]) and those using the FDT. Comparison of the results for both sets show lower correlations for Set 1, but identical results for the more meaningful RMSE.

		BV/TV		Tb.Th*		Tb.Sp*	
Ref. results mean ± SD (%)		0.08 ± 0.02 (26%)		122 µm ± 21 µm (17%)		944 µm ± 133 µm (14%)	
		RMSE in %	R^2	RMSE in %	R^2	RMSE in %	R^2
Set 1	Stereol.	19	0.49 **	16	0.19 ○	12	0.25 *
	Fuzzy	eq. to stereol.		12	0.56 ***	10	0.51 **
Ref. results mean ± SD (%)		0.19 ± 0.06 (32%)		324 µm ± 59 µm (18%)		1069 µm ± 205 µm (19%)	
		RMSE in %	R^2	RMSE in %	R^2	RMSE in %	R^2
Set 2	Stereol.	20	0.67 ***	17	0.19 ○	11	0.72 ***
	Fuzzy	eq. to stereol.		13	0.52 **	10	0.76 ***

Levels of significance: ○ : $p < 0.1$, * : $p < 0.05$, ** : $p < 10^{-2}$, *** : $p < 10^{-3}$

Table 1: Linear regression results for variables BV/TV, Tb.Th*, and Tb.Sp*.

Conclusions

Stereological and fuzzy methods, both estimate Tb.Sp* with RMS-errors substantially smaller than the sample SD. The fuzzy approach yields better estimates for Tb.Th*. This demonstrates that microstructural information can be extracted from the HRCT images under in vivo conditions with acceptable residual accuracy errors. Experiments with different membership functions give evidence that Tb.Th* estimation can be improved in future. Measurements with and without the abdominal phantom suggest that the slope of regression lines depend on image noise.

Acknowledgments: This work was supported by *The European Regional Development Fund* (ERDF) and by *Innovationsstiftung Schleswig-Holstein* (ISH) under Grant 2005-41T.

[GTN+07] Christian Graeff, Wolfram Timm, Thomas N Nickelsen, Jordi Farrerons, Fernando Marn, Clare Barker, and Claus C Glüer. Monitoring teriparatide-associated changes in vertebral microstructure by high-resolution ct in vivo: Results from the eurofors study. *Journal of Bone and Mineral Research*, 22(9):1426–1433, 2007.

[LR99] A. Laib and P. Rüegsegger. Calibration of trabecular bone structure measurements of in vivo three-dimensional peripheral quantitative computed tomography with 28-microm-resolution microcomputed tomography. *Bone*, 24(1):35–39, 1999.

[SW04] P.K. Saha and F.W Wehrli. Measurement of trabecular bone thickness in the limited resolution regime of in vivo mri by fuzzy distance transform. *IEEE Transactions Medical Imaging.*, 23(1):53–62, 2004.